The uptake of tau amyloid fibrils is facilitated by the cellular prion protein and hampers prion propagation in cultured cells

De Cecco, Elena ; Celauro, Luigi ; Vanni, Silvia ; Grandolfo, Micaela ; Bistaffa, Edoardo ; Moda, Fabio ; Aguzzi, Adriano ; Legname, Giuseppe

Abstract: Tauopathies are prevalent, invariably fatal brain diseases for which no cure is available. Tauopathies progressively affect the brain through cell-to-cell transfer of tau protein amyloids, yet the spreading mechanisms are unknown. Here we show that the cellular prion protein (PrPC) facilitates the uptake of tau aggregates by cultured cells, possibly by acting as an endocytic receptor. In mouse neuroblastoma cells, pull-down experiments revealed that tau amyloids bind to PrPC; Confocal images of both wild-type and PrPC - knockout N2a cells treated with fluorescently labelled synthetic tau fibrils showed that the internalization was reduced in isogenic cells devoid of the gene encoding PrPC. Pre-treatment of the same cells with antibodies against N-proximal epitopes of PrPC impaired the binding of tau amyloids and decreased their uptake. Surprisingly, exposure of chronically prion-infected cells to tau amyloids reduced the accumulation of aggregated prion protein; this effect lasted for more than 72 hours after amyloid removal. These results point to bidirectional interactions between the two proteins: whilst PrPC mediates the entrance of tau fibrils in cells, PrPSc buildup is greatly reduced in their presence, possibly because of an impairment in the prion conversion process.

DOI: https://doi.org/10.1111/jnc.15040

DR. ELENA DE CECCO (Orcid ID : 0000-0002-0148-2596)
DR. SILVIA VANNI (Orcid ID : 0000-0003-1192-7322)

Article type : Original Article

The uptake of tau amyloid fibrils is facilitated by the cellular prion protein and hampers prion propagation in cultured cells

Elena De Cecco[1*], Luigi Celauro[1], Silvia Vanni[1], Micaela Grandolfo[1], Edoardo Bistaffa[2], Fabio Moda[2], Adriano Aguzzi[3], Giuseppe Legname[1,4†].

[1] Laboratory of Prion Biology, Department of Neuroscience, Scuola Internazionale Superiore di Studi Avanzati (SISSA), Trieste, Italy.

[2] Fondazione IRCCS Istituto Neurologico Carlo Besta, Unit of Neurology 5 and Neuropathology, Milan, Italy.

[3] Institute of Neuropathology, University Hospital of Zürich
Schmelzbergstrasse 12, CH-8091 Zürich, Switzerland.

[4] ELETTRA Sincrotrone Trieste S.C.p.A, Basovizza, Trieste, Italy.

Running title: Tau K18 amyloids enter cells through binding to PrP^C and block prion propagation.

* Current affiliation: Institute of Neuropathology, University Hospital of Zürich, Schmelzbergstrasse 12, CH-8091 Zürich, Switzerland

This article has been accepted for publication and undergone full peer review but has not been through the copyediting, typesetting, pagination and proofreading process, which may lead to differences between this version and the Version of Record. Please cite this article as doi: 10.1111/JNC.15040

†Correspondence should be addressed to: Giuseppe Legname, Laboratory of Prion Biology, Department of Neuroscience, Scuola Internazionale Superiore di Studi Avanzati (SISSA), Trieste, Italy. Email: legname@sissa.it. Phone number: +39 0403787715

Keywords: prion protein, tau, prion propagation, internalization, scrapie

Abstract

Tauopathies are prevalent, invariably fatal brain diseases for which no cure is available. Tauopathies progressively affect the brain through cell-to-cell transfer of tau protein amyloids, yet the spreading mechanisms are unknown. Here we show that the cellular prion protein (PrP^C) facilitates the uptake of tau aggregates by cultured cells, possibly by acting as an endocytic receptor. In mouse neuroblastoma cells, pull-down experiments revealed that tau amyloids bind to PrP^C; Confocal images of both wild-type and PrP^C - knockout N2a cells treated with fluorescently labelled synthetic tau fibrils showed that the internalization was reduced in isogenic cells devoid of the gene encoding PrP^C. Pre-treatment of the same cells with antibodies against N-proximal epitopes of PrP^C impaired the binding of tau amyloids and decreased their uptake. Surprisingly, exposure of chronically prion-infected cells to tau amyloids reduced the accumulation of aggregated prion protein; this effect lasted for more than 72 hours after amyloid removal. These results point to bidirectional interactions between the two proteins: whilst PrP^C mediates the entrance of tau fibrils in cells, PrP^{Sc} buildup is greatly reduced in their presence, possibly because of an impairment in the prion conversion process.

List of abbreviations

3D: three-dimensional
Aß: amyloid-ß protein
AD: Alzheimer's disease
AFM: Atomic Force Microscopy
CNS: Central Nervous System
HPSGs: heparan sulfate proteoglycans
mGluR5: metabotropic glutamate receptor 5
N2a: Neuro-2a cell line
PK: proteinase K
PrP^{C} : cellular prion protein
PrP^{Sc} : scrapie prion protein
RRID: Research Resource Identifier
sCJD: sporadic CJD
SNpc: substantia nigra pars compacta
ThT: Thioflavin T
TEM: Transmission Electron Microscopy

Introduction

Tauopathies are a clinically heterogeneous group of diseases that affect many different anatomic regions. Their common trait is the ordered aggregation of misfolded and hyperphosphorylated tau

protein within neurons of the central nervous system (CNS). These aggregates have the morphology of fibrils and the tinctorial property of amyloid, i.e. they can be stained by Congo red and thioflavin T.

Several *in vitro* and *in vivo* studies showed that, at least to some extent, tau amyloids are able to recruit and seed the aggregation of the endogenous protein, therefore initiating the spreading from neuron to neuron (Khlistunova *et al.* 2006; Mirbaha *et al.* 2015; Holmes *et al.* 2014; Sanders *et al.* 2014; Falcon *et al.* 2015; Clavaguera *et al.* 2009; Clavaguera *et al.* 2013; Iba *et al.* 2015; Guo & Lee 2011). These findings, together with the observation that tauopathies progress in the CNS along predictable, neuroanatomically connected circuits (Braak & Braak 1991), led to the hypothesis that they might share some specific features with another group of neurodegenerative diseases, prion disorders. Unlike for prions, tau amyloids do not seem to undergo a fully infectious cycle, and horizontal propagation of tauopathies has not been demonstrated. Hence, tau aggregates are now considered to be "prion-like" proteins, or "prionoids" (Aguzzi 2009), along with α-synuclein and amyloid-β.

Cell-to-cell transfer of tau aggregates is mediated by several mechanisms (endocytosis, receptor-mediated endocytosis, macropinocytosis, tunneling nanotubes) (Holmes *et al.* 2013; Frost *et al.* 2009; Wu *et al.* 2013) that contribute to various extent to the propagation of the amyloids between cells. While some of these pathways are exclusive for tau, some others are exploited also by other neurodegeneration-related proteins. For example, α-synuclein is also thought to be transported along tunneling nanotubes (Tardivel *et al.* 2016).

Recent evidence proposes that the cellular prion protein (PrP^C) might underlie the progression of several distinct neurodegenerative disorders (Resenberger *et al.* 2011), both promoting the spreading of the misfolded proteins and mediating their neurotoxic effects. Indeed, the presence of PrP^C on the cell membrane is essential for the progression of prion disorders, and may be involved in the Aβ-associated neurotoxicity in Alzheimer's disease (AD) (Resenberger *et al.* 2012; Um *et al.* 2012), although the latter finding remains controversial (Calella *et al.* 2010).

In the case of Parkinson's disease, PrP^C may influence its pathogenesis in two ways: by acting as a receptor for α-synuclein aggregates that facilitates their internalization in healthy cells, and by mediating their toxic effects through the activation of a signaling cascade (Aulic *et al.* 2017; Ferreira *et al.* 2017). Interestingly, both Aβ- and α-synuclein-associated detrimental effects of PrP^C, as well as those of bona fide prion diseases, proceed through the activation of the mGluR5 receptor and fyn kinase, corroborating the hypothesis of a common mechanism (Um *et al.* 2012; Ferreira *et al.* 2017; Goniotaki *et al.* 2017).

Interestingly, targeting PrP^C with antibodies reduces the impairment of long-term potentiation caused by soluble forms of tau, therefore suggesting a role for the prion protein also in the progression of tauopathies (Ondrejcak *et al.* 2018; Ondrejcak *et al.* 2019). Since tau fibrils are mainly intracellular, it is worth investigating if PrP^C is involved in the uptake process of the aggregates, as it happens in the case of α-synuclein.

In the present study, we report that PrP^C expression enhances the entry of tau fibrils into mouse neuroblastoma cells. Conversely, blocking PrP with antibodies reduced the number of internalized fibrils. These findings suggest that impairing the binding of the fibrils to PrP^C might not only to ameliorate synaptic dysfunctions, but also impair the spreading of the aggregates to neighboring neurons. Most surprisingly, we discovered that tau fibrils interfere with PrP^{Sc} accumulation in prion-infected cell lines. We show that the addition of tau K18 amyloids to cultured cells causes a rapid and drastic decrease in PrP^{Sc} . We found that the treatment increases the α-cleavage of PrP^C into the neuroprotective fragments N1 and C1, thus depleting the pool of misfolding-prone protein and impeding prion conversion.

Materials and methods

This study was not pre-registered. No blinding was performed.

Ethical statement

Institutional ethical was not required for this study.

Production and fibrillization of recombinant tau K18

Expression and purification of recombinant tau K18 fragment were performed as previously described (Barghorn *et al.* 2005). *In vitro* fibrillization reactions were prepared in a 96-well black plate with transparent bottom (BD Falcon) in a final volume of 200 µL per well. Fibrillization reaction was composed as follows: tauK18 0.5 mg/mL, heparin 10 µg/mL, DTT 0.1 mM, PBS 1X pH 7.4. Due to its toxicity to cultured cells, 10 µM Thioflavin T was added only in 4 wells that were used to monitor the aggregation reaction in real-time. Each well contained also a 3-mm glass bead (Sigma). The plate was covered with sealing tape (Fisher Scientific) and incubated at 37°C under orbital shaking (50 seconds of shaking at 400 rpm followed by 10 seconds of rest) on

FLUOstar Omega (BMG Labtech) microplate reader. Fluorescence was monitored every 30 minutes by bottom reading at 444 nm of excitation and 485 nm of emission. For cell culture experiments, fibrillization was perfomed as described above but in absence of ThT. The reaction was stopped after 15 hours, when fluorescence reached plateau. Newly formed aggregates were pelleted by ultracentrifugation (55000 rpm for 1 hour at 4°C), resuspended in an equal volume of sterile PBS and stored at -20°C. Before use, aliquots were thawed and sonicated for 5 minutes in a sonicator Misonix s3000 at 250 W.

AFM and TEM analysis

AFM analysis was performed in tapping mode. 10 µL of fibril solution was deposited onto a freshly cleaved piece of mica and left to adhere for 30 min. Samples were then washed with distilled water and blow-dried under a flow of nitrogen. Images were collected at a line scan rate of 0.5-2 Hz in ambient conditions. The AFM free oscillation amplitudes ranged from 25 nm to 40 nm, with characteristic set points ranging from 75% to 90% of these free oscillation amplitudes. AFM data were analysed with Gwyddion (gwyddion. net).

For TEM analysis, 10 µL of fibrils solution was dropped onto 200-mesh Formvar-carbon coated nickel grids (Electron Microscopy Sciences) for 20 min and the remaining drop was blotted dry using Whatman filter paper. Subsequently, the samples were stained with 25% Uranyl Acetate Replacement (UAR, Electron Microscopy Sciences) for 10 min. The staining solution was removed using Whatman filter paper and the grids were air-dried for 5 min before the analyses. Amyloid samples were visualized using a FEI Tecnai Spirit Transmission Electron Microscope operating at 120 kV and equipped with an Olimpus Megaview G2 camera.

Cell culture

Mouse neuroblastoma cells N2a were kindly provided by Prof. Chiara Zurzolo (Unité de traffic membranaire et pathogenèse, Institute Pasteur, Paris, France). N2a *Prnp*$^{-/-}$ cells were kindly provided by professor Gerold Schmitt-Ulms (Tanz Centre for Research in Neurodegenerative Diseases, University of Toronto, Toronto, Ontario, Canada), for which they used the CRISPR-Cas9-Based Knockout system to ablate the expression of PrP protein (Mehrabian *et al.* 2014). ScN2a cells are clones persistently infected with the RML prion strain as described by Prusiner's group (Butler *et al.* 1988) or with the 22L prion strain. Cells were grown at 37°C and 5% CO2, in

minimal essential medium (MEM) + glutamax (Thermo Fisher Scientific Inc.), supplemented with 10% fetal bovine serum, 1% non-essential aminoacids, and 100 units/ml penicillin and 100 µg/ml streptomycin. The cell lines are not listed as commonly misidentified cell lines by the International Cell Line Authentication Committee. The cells were kept in culture for 6 passages maximum.

TauK18 fibrils treatment in cell lines

TauK18 amyloids were added to the cell culture medium of N2a, N2a *Prnp*$^{-/-}$ and ScN2a cell lines in 10 cm plates, and incubated for a variable amount of time according to the specific experimental setting (ranging from 1 day to 6 days). For the evaluation of PrP^{Sc} clearance in ScN2a cell line, cells were split and maintained for five additional passage in fibrils-free cell culture medium. For fluorescence quantification of amyloids internalization, cells were plated in 24-wells plates on 12 mm coverslips and incubated with Alexa488-labeled fibrils for 24 – 72 hours. Labelling with Alexa-488 succinimidyl ester (ThermoFisher) was performed according to manufacturer's instructions. Unbound dye was removed by subsequents steps of dyalisis.

Pull-down assay

N2a cells were lysed in lysis buffer (0.1% NP40, 50 mM TrisHCl pH 8, 150 mM NaCl) containing one tablet of Complete™ ULTRA Tablets, EDTA-free, glass vials Protease Inhibitor Cocktail (Roche). Total protein content was quantified using bicinchoninic acid protein (BCA) quantification kit (Pierce). For inhibition of the interaction using POM12, N2a cell lysate was incubated for 1 hour with POM12 (15 µg/mL) at 37°C. 1 mg of total protein content was diluted in lysis buffer to a final volume of 500 µL, then biotinylated tauK18 fibrils were added to a final concentration of 2 µM. Samples were left standing on a rotor wheel overnight at 4°C. The day after, 30 µL were collected from each sample and stored at -20°C for further analysis (input samples). 30 µL of neutravidin bead slurry (NeutrAvidin Agarose Resins, ThermoFisher Scientific) were added to each tube, and the samples were incubated on the rotor wheel at 4°C for 4 hours. To precipitate the beads, the samples were centrifuged at 4°C for 2 minutes at 2000 rpm, the pellet was washed with three subsequent steps of resuspension in lysis buffer and centrifugation, and finally resuspended in 20 µL of Laemmli loading buffer. Samples were boiled for 10 minutes and centrifuged at 13000 rpm for 1 minutes to detach and pellet the beads, respectively. The supernatants were collected and stored at -20°C for further analysis.

Trypan blue quenching of non-internalized fibrils and imaging

30000 cells were cultured on each coverslip and treated with different concentrations of Alexa488-labeled tau K18 amyloids. Before fixation, cells were washed twice with sterile PBS and incubated for 5 minutes with a sterile 1:1 solution of Trypan Blue : PBS. As shown by Karpowicz et al.(Karpowicz *et al.* 2017), Trypan Blue quenches green fluorescence through an energy-transfer mechanism, but being unable to enter alive cells, only the fluorescence coming from non-internalized fibrils is quenched.

Cells were then rinsed three times with sterile PBS and fixed for 10 minutes with 4% paraformaldehyde/PBS. After three washing steps, cells were permeabilized for 5 minutes with 0.2% Triton X-100/PBS, rinsed again with PBS and incubated for 1 hour with HCS Blue Cell Mask (ThermoFisher Scientific) diluted 1:1000, a specific dye that labels the whole cell cytoplasm. Coverslips were mounted in Fluoromount-G™ (ThermoFisher Scientific) and stored at 4°C for confocal fluorescence microscopy. Images were acquired using a Nikon confocal microscope (Nikon C1).

Inhibition of tau K18 amyloids internalization using POM monoclonals

Anti-PrP^C monoclonal antibodies were kindly provided by Prof. Adriano Aguzzi (Institute of Neuropathology, University of Zürich) (Polymenidou *et al.* 2008). N2a cells plated on coverslips were pre-treated with each POM antibody (15 µg/mL) for 1 hour at 37°C, followed by incubation with Alexa488-labeled tauK18 fibrils for 24 hours. Coverslips were processed and mounted as described above. To check the binding of POM antibodies to membrane PrP^C, cells treated with POM antibodies for 1 hour were fixed with 4% paraformaldehyde:PBS for 10 minutes, then blocked with 2% FBS for 30 minutes and incubated with Alexa594-conjugated goat anti-mouse IgG diluted 1:200 for 1 hour.

Uptake quantification

The uptake quantification was performed in blind on a total of four hundred cells in three independent experiments. Random fields on each coverslip were captured at 63x magnification (digital zoom 3X) using Nikon C1 confocal microscope. Images were acquired as stacks of 30 - 40 optical sections of 0.27 µm, 526 x 526, and subsequently deconvolved with a 3D deconvolution algorithm (in blind) of the NIS Elements software. Deconvolution was applied only to the green channel, as it allows a better separation of the green dots representing the fibrils. Deconvolved images were analysed using Volocity Workstation (PerkinElmer, version 4.1) and

internalized fibrils were counted using a home-made script which intersects the objects recognized in the green channel with the 3D reconstruction of the cellular volume (blue channel). To discriminate the signals corresponding to fibrils from the background, we used the volume of a single monomer of synuclein as a threshold. Synuclein is very similar to tau K18 in terms of molecular weight and unfolded structure. The volume of a monomer in its multiple conformations was obtained from Zhang et al. (Zhang *et al.* 2018)

Membrane immunostaining of PrP^C

N2a cells seeded on coverslips were treated for 24 – 72 hours with 2 µM of tau K18 amyloids. Surface staining of PrP^C was performed as described in Stincardini et al. (Stincardini *et al.* 2017). Cells were incubated with W226 antibody diluted 1:250 in Opti-MEM (Life Technologies) for 15 minutes at 4°C, followed by washing in PBS and fixation with 4% paraformaldehyde:PBS for 10 minutes. Coverslips were then washed three times with PBS, incubated with blocking solution (2% FBS in PBS) for 30 minutes and incubated with Alexa-594 conjugated goat anti-mouse IgG (Invitrogen) diluted 1:200 in blocking solution. Finally, nuclei were counterstained with DAPI (1:1000). Coverslips were mounted in Fluoromount-G™ (ThermoFisher Scientific) and stored at 4°C. Images were acquired with Nikon C1 confocal at 63x magnification, both as 2D-images of medial planes and series of 30-40 optical sections (z-step = 0.27 µm, 526x526).

Quantification of membrane staining

Quantification of membrane staining was performed with Volocity Workstaton (PerkinElmer) on 2D images. Image segmentation consisted first of nuclei identification by the DAPI signal, and selection of the region of interest by the Alexa-594 signal. Mean fluorescence intensity values of Alexa594-conjugated anti-PrP antibody were measured for more than 600 objects per coverslip, and weighted averages were calculated in order to identify any difference between untreated and treated samples. To confirm that 2D quantification is representative of the situation of the whole cell membrane, the same 3D analysis was performed on a number of z-stacks from both untreated and treated samples.

Western blotting

Total protein contents of N2a untreated and treated with 2 µM of tau K18 amyloids were quantified using bicinchoninic acid protein (BCA) quantification kit (Pierce). Fifty µg of total

proteins were used and additioned with 5X loading buffer in a ratio 1:5. The samples were boiled at 100°C for 10 minutes, loaded onto a 12% Tris-Glycine SDS-PAGE gel and transferred onto Immobilon P PVDF membranes (Millipore) for 2 hours at 4°C. The membrane was blocked in 5% non-fat milk and incubated overnight at 4°C with human anti-PrP antibodies (D18 1:1000, W226 1:1000, SAF34 1:1000). The membrane was washed three times with TBS buffer additioned with 0.2% Triton X-100, incubated for 45 minutes at room temperature with goat anti-human IgG conjugated with horseradish peroxidase and developed with the enhanced chemiluminescent system. After the acquisition, the membrane was incubated for 30 minutes at room temperature with anti β-actin (1:10000, Sigma-Aldrich), which is used as a normalizer. Images were acquired with Uvitec Alliance (Cambridge) and densitometric analysis was performed using Uviband analysis software. Data are expressed as mean ± SD, and the values of the controls are adjusted to 100%. For tau fibrils detection, the membrane was probed with anti-4R tau RD4 antibody diluted 1:1000.

Total RNA extraction and RT-PCR analysis

The total RNA extraction was performed using PureLink RNA MiniKit with TRIzol® Reagent (Life Technologies) following the manufacturer's instruction. Briefly, control cells and cells treated with tauK18 fibrils were washed twice with PBS 1X and lysed using the TRIzol® Reagent. Following RNA isolation, a DNase I digestion was performed using 1 unit of enzyme per µg RNA for 15 min at room temperature, and RNA clean-up was implemented using RNeasy spin columns following the instructions. RNA concentration was determined using the NanoDrop system (Thermo Scientific). First-strand cDNA was synthesized using 3 µg of total RNA in a 20 µL reverse transcription reaction (RT+ samples) mixture following the instructor manual. For each sample a non-retrotranscribed sample was carried along as a negative control (RT− sample).

The cDNA was diluted to 10 ng/µL final concentration prior to Real-Time PCR reactions. 1 ng of cDNA was added to the reaction mix including 2× iQ™ SYBR® Green Supermix (Bio-Rad Laboratories, Inc.), 400 nM of the corresponding forward and reverse primer (Sigma), and quantified in technical duplicates on an iQ5 Multicolor Real-Time PCR Detection System (Bio-Rad Laboratories, Inc.).

After initial denaturation for 3 min at 95°C, 45 cycles were performed at 95°C for 10 sec and 60°C for 1 min. Differential gene expression of was normalized to GAPDH expression. RT– controls were included in the plates for each primer pair and sample. The relative expression ratio was calculated using the ΔΔCT method [299]. Significance was calculated with the unpaired student t-test ($p < 0.05$). The primers used for RTqPCR reactions are listed in Table 1.

Gene	**Chromosome**	**Primer sequence**	**Amplicon length (bp)**
GAPDH	11	F: CCTGCACCACCAACTGCTTA R: CTGTCACCTTCACCGTTCC	74
PRNP	2	F: GAGACCGATGTGAAGATGATGGA R: TAATAGGCCTGGGACTCCTTCTG	80

Table 1.

PNGase F treatment

PNGase F treatment (New England Biolabs) was performed on control and K18-treated ScN2a cell lysates. Twenty µg of total proteins were incubated with 1 µL of Glycoprotein Denaturating Buffer (10X) and water to reach a total reaction volume of 10 µL, then the mix was heated at 100 °C for 10 minutes to denature the proteins. The solution was chilled on ice and centrifuged for 10 seconds, then additioned with 2 µl of GlycoBuffer 2 (10X), 2 µl of 10% NP-40, 6 µl of H2O and 1 µl of PNGase F. The solution was incubated overnight at 37°C. Deglycosylated proteins were then analysed by Western Blot.

Statistical Analysis

All statistical analysis were performed using GraphPad Prism software (version 7.0a) (RRID: SCR_002798). Values were expressed as mean ± standard deviation (SD). For the quantification of the internalized fibrils, the ROUT test for the identification of outliers was performed. As the sample sizes exceeded n=30, according to the Central Limit Theorem, we assumed a gaussian distribution of our data, and used the Student's T test with Welch correction for the comparison of the two groups. The same analysis was repeated also using Mann-Whitney non-parametric test. Comparisons of multiple groups versus a control group were evaluated with one-way ANOVA (Dunnett's multiple comparisons test). The differences were considered statistically significant at $P < 0.05$.

Results

The presence of PrP^C on the cell membrane facilitates the uptake of tau K18 amyloids.

To test whether PrP^C expression affects in some way the entrance of tau K18 amyloids in cells, we compared the number of internalized fibrils in wild-type N2a cells expressing physiological levels of the prion protein to that of N2a cells ablated for PrP^C (N2a *Prnp*$^{-/-}$, obtained using the Crispr-Cas9 Based Knockout system (Kessels *et al.* 2010)). Synthetic amyloids were prepared through an *in vitro* fibrillization process starting from recombinant tau K18 protein (Supplementary Fig. S1 a-d). The purity of the protein was checked by SDS-PAGE (Supplementary Fig. S1a). The resulting amyloids were structurally characterized by atomic force microscopy (AFM) before and after a round of 5 minutes of sonication (Supplementary Fig. S2 a-c). As visible from AFM images, the sonication process both broke the amyloids into more homogeneous smaller species, and disrupts the big aggregates formed as a consequence of the deposition of the sticky fibers in the wells. Short amyloid aggregates were indeed shown to be internalized more easily by cultured cells (Aulic *et al.* 2014). AFM data were then complemented by TEM analysis (Supplementary Fig. S2 d-e). Therefore, in all following experiments we used exclusively the sonicated preparations of tau K18 amyloids. We performed proteolytic digestion followed by Western blotting, and found that the sonicated preparation of tau fibrils was partially resistant to proteinase K (Supplementary Fig. S1e). We then assessed the cytotoxicity of different concentrations of the fibrils preparations on all the mouse N2a cell lines used in this study for up to 72 hours (Supplementary Fig. S3). We did not detect any significant toxicity after exposure to tau K18 amyloids. To quantify the number of internalized fibrils in N2a cells, we used confocal microscopy of Alexa 488-labelled tau K18 amyloids. Fluorescent labelling of tau K18 amyloids, followed by incubation in cell culture medium and quenching of non-internalized material with the vital dye Trypan Blue (Karpowicz *et al.* 2017), allows a more precise quantification of the amyloids by reducing the background signal associated with the use of antibodies. Uptake experiments on wild-type N2a showed that, in our model system and in our experimental conditions, tau K18 amyloids are spontaneously endocytosed in a time- and concentration dependent manner (Supplementary Fig. S4). Higher concentrations (2 μM) required only 24 hours to be taken up by the cells, while in the case of lower concentrations (0.5 μM), 72 hours were needed in order to have 100% of cells positive for aggregates.

To assess the contribution of PrP^C to the uptake, we treated N2a and N2a *Prnp*$^{-/-}$ with 2 μM of 488-tau K18 amyloids fibrils for 24 hours, and measured the number of internalized amyloids. We found that wild-type N2a cells took up an average number of 77 ± 41 fibrils per cell compared to the 49 ± 36 fibrils of N2a *Prnp*$^{-/-}$ ($p<0.0001$, Fig. 1A and B). The difference in the number of

internalized tau K18 amyloids between wild-type N2a and N2a *Prnp*$^{-/-}$ cells exhibited the same trend in three experiments performed with different clones of cells and independent preparations of 488-tau K18 amyloids. Moreover, we repeated the same experiment varying the concentration of tau K18 amyloids and the incubation time, and found very similar results in terms of differential internalization, therefore confirming the robustness of our findings (Supplementary Fig. S6).
As cells change their volume during the progression of the cell cycle (Boucrot & Kirchhausen 2008), we analyzed the cell dimensions in order to rule out the possibility that the higher internalization of tau K18 amyloids by N2a cells might be artifactual (Supplementary Fig. S5). Indeed, the number of internalized tau K18 amyloids and the cell volume are positively correlated (Supplementary Fig. S5a). No difference was found in the cell volumes between N2a and N2a *Prnp*$^{-/-}$ used in the three experiments shown in Fig. 1A and B. (Supplementary Fig. S5b).

Tau amyloids bind to PrP^{C} and enter cells through an energy-dependent mechanism.

Previous works showed that both Aβ and α-synuclein amyloids bind to PrP^{C} in order to exert their detrimental effects and, in the case of synuclein, to gain cell entrance (Resenberger *et al.* 2012; Aulic *et al.* 2017). Therefore, we hypothesized that a similar mechanism might underlie also the uptake of tau fibrils. To better define the molecular interaction between the two proteins, we performed a pull-down assay in which biotinylated tau amyloids were used as baits to precipitate PrP^{C} from N2a cell lysate. The data demonstrate that tau K18 amyloids bind to PrP^{C} *in vitro* (Fig. 1C). Evidence of the interaction between the cellular prion protein and monomeric forms of tau is already present in literature (Han *et al.* 2006); however, no previous studies have been conducted using fibrillar aggregates of tau. As previous reports claim that PrP^{C} interacts with binding partners through its N-terminal tail (Fluharty *et al.* 2013; Aulic *et al.* 2017), we tried to inhibit the interaction with tau K18 amyloids by pre-incubating N2a cell lysate with POM12 antibody targeting the N-proximal portion (the octapeptide GQPHGGG/SW of the octarepeat region). Lane 5 of Fig. 1D shows that when tau K18 amyloids are incubated with POM12-treated N2a lysate and pulled down, no signal is visible after detection with anti-PrP antibody, confirming that the interaction has indeed been impaired.
The binding of the fibrils to PrP^{C} suggests that the internalization might occur through an energy-dependent, receptor-mediated endocytic pathway rather than via channel diffusion. To test this hypothesis, we incubated N2a and N2a *Prnp*$^{-/-}$ cells with tau fibrils for 6 hours either at 37°C or at 4°C, which blocks all ATP-dependent processes. As expected, wild-type N2a exhibited a greater uptake of tau K18 amyloids under normal culture conditions, with respect to their counterpart not expressing PrP^{C} (Fig. 1E). However, at lower temperature (4°C) we observed an almost complete

inhibition of the internalization for both cell types, regardless of their genetic background (Fig. 1F), indicating an ATP-dependent mechanism required for the internalization of tau K18 amyloids.

Finally, we validated the contribution of the cellular prion protein to tau K18 amyloids internalization by targeting PrP^C with monoclonal antibodies directed against the N-proximal portion (the aforementioned POM12 antibody), the amino acids 95-100 of the hydrophobic region (POM3 antibody) and a conformational epitope spanning amino acids 121-134 and 218-221 of the C-terminal domain (POM4 antibody) (Polymenidou *et al.* 2008). Both POM12 and POM3 decreased the uptake of tau K18 amyloids to a level similar to that of N2a *Prnp*$^{-/-}$cells (Fig. 1G). This is in agreement with the findings of a recent study revealing the toxic effects of soluble tau aggregates are reverted when at least one of these two PrP^C regions are blocked (Ondrejcak *et al.* 2018). On the contrary, targeting the C-terminal domain of PrP^C did not result in any change in the amount of internalized tau K18 amyloids (Fig. 1G).

Figure 1. Uptake of tau K18 amyloids in mouse neuroblastoma cell lines. (A) Confocal microscopy images showing the orthogonal views of the central section of the 3D Z-stack for N2a and N2a *Prnp*$^{-/-}$ (in blue) treated with tau K18 fibrils (in green) for 24 hours. (B) Scatter plot showing the distribution of the number of internalized fibrils in N2a and N2a *Prnp*$^{-/-}$ cells. A total of three hundred cells were counted in blind in n= 3 experiments with independent cell culture and fibrils preparations . Numbers on top indicate the average number of internalized fibrils. Data were evaluated with unpaired T-test with Welch's correction. Statistical analysis is indicated as: * = $p < 0.05$, ** = $p < 0.01$, *** = $p < 0.001$, **** = $p < 0.0001$.. (C) Western Blot of pulled down samples (lanes 1-3) and input samples (lanes 4-6). Lane 1: K18 fibrils only; lane 2: N2a lysate only; lane 3: K18 fibrils and cell lysate. Lane 4: K18 fibrils only; lane 5: N2a cell lysate only; lane 6: K18 fibrils and cell lysate. The membrane was probed with human anti-PrP^C antibody D18 and with anti-biotin to visualize tau K18 amyloids. n= 3 experiments with independent cell culture and fibrils preparations. (D) Western Blot of pulled down samples and input samples. Lane 1: N2a lysate only; lane 2: K18 fibrils only; lane 3: K18 fibrils and cell lysate. Lane 4: N2a cell lysate + POM12; lane 5: N2a cell lysate + POM12 + tau K18 amyloids. The membrane was probed with human anti-PrP^C antibody D18 and with anti-biotin to visualize tau K18. (E) and (F) Internalization of tau K18 amyloids by N2a and *N2a Prnp*$^{-/-}$ cells at 37°C (E) and 4°C (F). Images were acquired using a confocal microscope as series of Z-stacks and the analysis was carried out in 3D. Images show

one of the central sections of the stack, both as separate channels and as a merge of the two channels. n= 3 experiments with independent cell culture and fibrils preparations. (G) Scatter plots representing the distribution of internalized fibrils in N2a cells treated only with tau K18 fibrils and in N2a that were pre-treated with different anti-PrP^C antibodies. Numbers on top indicate the average number of internalized fibrils. Data were evaluated with unpaired T-test with Welch's correction. Statistical analysis is indicated as: *= $p<0.05$; **= $p<0.01$; ***= $p<0.001$.

Tau fibrils induce an increase of the endogenous prion protein that localizes on the cell membrane.

To better characterize the mutual relationship between tau amyloids and PrP^C, we asked if the treatment with tau K18 fibrils has any effect on the endogenous levels of PrP^C at different timepoints (Fig. 2, A-B). After 72 hours of incubation, we found an increase of around 60% of the total PrP^C level in N2a cells, while at 24 and 48 hours no changes were detected. This effect was dependent on the presence of the aggregates in the culture medium, because when treated cells are passaged and kept in fibrils-free medium, PrP^C level went back to basal levels (Fig. 2A). The observed variation in total PrP^C occurs only at the protein level, since we did not find any increase in the levels of *Prnp* mRNA after tau K18 amyloids treatment (Supplementary Fig. S7). Immunofluorescence stainings of PrP^C in untreated and tau-treated N2a cells revealed that around 35% of the excess PrP^C was localized on the plasma membrane (Fig.3). The increase in PrP-associated fluorescence levels occured only after 72 hours of incubation with tau amyloids, in agreement with Western Blot data (Fig. 3). N2a cells treated with 10 µM chlorpromazine, which is known to decrease the amount of PrP^C on the surface of the cells (Stincardini *et al.* 2017), were used as control to assess the validity of the experimental method (Supplementary Fig. S8).

Figure 2. Exposure of N2a cells to tau K18 fibrils induces an increase of the endogenous prion protein. (A) Western blot analysis of N2a cells treated with 2 µM of tau K18 fibrils for 24, 48 and 72 hours and of the first passage of N2a treated for 72 hours. Membranes were probed with human anti-PrP antibody D18. (B) Quantification of three independent experiments. Data are represented as the percentage of total PrP relative to ß-actin. ß-actin is a loading control. Data are represented as mean ± SD. Data were evaluated by unpaired T-test. Statistical analysis is indicated as: n.s.= not significant; *= $p<0.05$; **= $p<0.01$; ***= $p<0.001$.

Figure 3. Exposure of N2a cells to tau K18 fibrils induces an increase of the endogenous prion protein. (A) Representative immunofluorescence images of untreated and treated N2a at three different timepoints. Membrane staining for PrP^C was performed at 4°C on alive cells using the W226 antibody. The magnified sections show a visible difference in the fluorescence intensity

associated to PrP^C between control cells and cells treated for 72 hours. In all the images, the green signal corresponds to Tau K18 amyloids and the red signal to PrP^C. (B) Scatter plot of the intensity of the PrP-associated membrane staining of treated N2a compared to control cells. The intensity values, which correlates with the levels of PrP on the membrane, is reported as the ratio between the average intensities of treated and control cells for each timepoint. Controls have been normalized to 1. The three values represent three independent experiments, in which 700 cells for each condition were analysed. Data have been evaluated with unpaired T-test. Statistical analysis is indicated as: n.s.= not significant; *= $p<0.05$; **= $p<0.01$; ***= $p<0.001$. (C) Orthogonal views of the central section of the 3D Z-stack for N2a control cells and N2a treated with K18 amyloids for 72 hours.

Tau amyloids lower PrP^{Sc} levels in cell lines infected with different prion strains

Although the process of prion conversion and PrP^{Sc} formation depends mainly on the presence of PrP^C, recent studies revealed that it can be affected by the concomitant presence of intracellular amyloids of other neurodegeneration-related proteins (Aulic *et al.* 2017). In the case of tau protein, this assumes clinical relevance as some cases were documented where prion pathology co-exists with tau deposits (Rossi *et al.* 2019; Piccardo *et al.* 2017; Ghetti *et al.* 1996). To assess the effect of tau fibrils on PrP^{Sc} levels, we exposed a neuroblastoma cell line persistently infected with RML prion strain (ScN2a RML) to two different concentrations of tau K18 amyloids and we analysed the PK-resistant PrP^{Sc} at different timepoints (Fig. 4A). The quantification of three independent experiments (Fig. 4B), showed that the time required for PrP^{Sc} clearance is dependent on the concentration of tau K18 amyloids. Indeed, cells treated with 5 μM tau K18 amyloids showed significantly less prions after 48 hours, while treating with a lower concentration of tau K18 amyloids (2 μM) required 72 hours to lead to a 50% decrease in prion burden. Although the highest concentration of tau K18 amyloid proved to be more effective in clearing PrP^{Sc} after 72 hours, we chose to use 2 μM for further experiments, as it gave more reproducible results. Immunofluorescence data (Fig. 4C) revealed that tau K18 amyloids are taken up by ScN2a cells, and they appear to co-localize with lysosomes (Supplementary Fig. S9). Next, we wondered if PrP^{Sc} levels could remain low upon passaging, even in the absence of tau fibrils. After a 72 hours-incubation with 2 μM of tau K18 amyloids, cells were kept in culture for 5 additional passages. (Fig. 5A, 5B, 5C). The prion load decreased after the treatment with the

amyloids and remained low through two subsequent passages (Fig. 5A and B), while monomeric K18 used as a control did not affect prion levels. However, although the reduction observed after the initial passages was quite pronounced, it was not maintained after the third passage without fibrils, where PrP^{Sc} levels rose again to their initial level (Fig. 4C). A longer incubation with the fibrils did not result in a complete clearance of PrP^{Sc}, since a weak signal was still present at passage 3 (Supplementary Fig. S10).

We tested the strain dependency of tau K18-induced clearance of PrP^{Sc} by repeating the treatment on ScN2a infected with the 22L prion strain (Figure 4C). Also in this case we reported a strong reduction in the PrP^{Sc} load after the administration of the fibrils, indicating that the mechanism activated by tau K18 is not affected by strain differences.

Taken together, these results show that tau K18 amyloids are able to clear PrP^{Sc} in cultured cells permanently replicating different prion strains, and that they have to be present in the cell culture medium in order to keep the prion burden low. This effect occurs probably through a direct interaction with either PrP^{C} or PrP^{Sc}. Since tau K18 amyloids interact with PrP^{C}, we hypothesized that the fibrils might bind and reduce the availability of PrP^{C} for PrP^{Sc}-induced conversion. Indeed, we found that the treatment with K18 fibrils promotes the α-cleavage of PrP^{C} with the formation of the N1 and C1 fragment, thus reducing the pool of PrP^{C} needed for the conversion (Fig. 5E).

Figure 4. Tau-induced PrP^{Sc} clearance in ScN2a RML cell line at different timepoints. (A) Western Blot analysis of PK-resistant PrP^{Sc} upon treatment with different concentrations of tau K18 amyloids at 24 hours, 48 hours and 72 hours. (B) Quantification of three independent experiments. Values are shown as a percentage of PK-resistant form relative to β-actin. β-Actin is a loading control. Data are represented as mean ± SD. Data were evaluated by one-way ANOVA with multiple comparisons. Statistical analysis is indicated as: *= $p < 0.05$, **= $p < 0.01$, ***= $p < 0.001$. (C) Confocal microscopy image showing the orthogonal views of the central section of the 3D Z-stack of ScN2a RML cells treated with 2 μM of tau K18 amyloids (in green) for 72 hours.

Figure 5. Clearance of PrP^{Sc} from prion-infected ScN2a cell lines after treatment with tau K18 amyloids. (A) Western blot analysis of PK-resistant PrP^{Sc} in ScN2a RML cell lysates upon

treatment with tau K18 amyloids for 3 days from the addition of the fibrils (passage 0) to passage 2. (B) Quantification of n=3 experiments with independent cell culture and fibrils preparations. Values are shown as a percentage of PK-resistant form relative to β-actin. β-Actin is a loading control. Data are represented as mean ± SD. Data were evaluated by one-way ANOVA with multiple comparisons. Statistical analysis is indicated as: *= $p < 0.05$, **= $p < 0.01$, ***= $p < 0.001$. (C) Western Blot analysis of further passaging of treated cells shown in (A), from passage 3 to passage 5. (D) Western blot analysis of PK-resistant PrP^{Sc} in ScN2a 22L cell lysates upon treatment with tau K18 amyloids for 3 days. (E) Electrophoretic pattern of PNGase F digested PrP in ScN2a control cells and cells treated with tau K18 fibrils. Solid black arrow shows the presence of C1 fragment recognized with C-terminal Ab (W226), while the broken black arrow indicates the absence of the bands when the membrane was probed with N-terminal antibody (SAF34).

Discussion

A number of reports claim that the role of the cellular prion protein in neurodegeneration is not limited to prion disorders, but extends also to the pathogenesis of Alzheimer's disease and synucleinopathies (Resenberger *et al.* 2011; Resenberger *et al.* 2012; Aulic *et al.* 2017; Urrea *et al.* 2017; Ondrejcak *et al.* 2018). Indeed, several reports indicate that PrP^C mediates the neurotoxicity of several protein aggregates (α-synuclein, amyloid β) in two different ways. Firstly, PrP^C was reported to act as a membrane receptor to facilitate their internalization(Ondrejcak *et al.* 2018; Chen *et al.* 2010; De Cecco & Legname 2018; Aulic *et al.* 2017). Secondly, PrP^C may function as a transducer of their detrimental effects through the activation of metabotropic glutamate receptors (Um *et al.* 2012; Abe & Bonini 2013).

Our study gives a more detailed insight into the molecular mechanisms of the interplay between tau and the prion protein, and points towards an alternative and complementary role of PrP^C in the pathogenic process of tauopathies. Indeed, as the involvement of PrP^C in the tau-induced toxicity and impairment of long-term potentiation seems to be assessed (Ondrejcak *et al.* 2018; Ondrejcak *et al.* 2019), we demonstrated that the interaction between the two proteins is deeper than expected, and extends also to the cell-to cell propagation of tau pathology.

First, we showed that sonicated tau K18 fibrils bind to PrP^C. The existence of an interaction between the two partners is the first mandatory step in the cascade of events leading to PrP^C-dependent internalization. Although there is proof of the interaction of the prion protein with monomeric full-length tau in the literature (Han *et al.* 2006), no experiments had been performed so far using synthetic aggregates. In addition, the existence of a direct interaction between PrPC and amyloid species is still an open question. Recently, La Vitola *et al.* (La Vitola *et al.* 2019) could not detect any binding between PrP^C and α-synuclein amyloids in hippocampal neurons and in mouse models. These results are in contrast with a full body of evidence pointing at this interaction as the first step in a cascade of events leading to amyloid-induced neurotoxicity and cellular internalization of α-synuclein aggregates (Aulic *et al.* 2017; Ferreira *et al.* 2017). Regarding tau, what we observed is in line with the findings of Ondrejcak *et al.* (Ondrejcak *et al.* 2018; Ondrejcak *et al.* 2019), as in both cases the direct targeting of PrP^C with antibodies reduced the internalization of tau amyloids and their effects on long-term potentiation, respectively. The negative results obtained by La Vitola might be due to the highly variable conformation of α-synuclein oligomers and to the fact that only one type of preparation was tested, as stated by the authors themselves. Moreover, oligomers are likely to be transient species in the process of aggregation, and as such to have a more heterogenous conformation. Since PrP^C appears to bind to β-sheet enriched regions, the different structural organization of the oligomers might account for the lack of binding. For this reason, we chose to use sonicated

tau fibrils throughout all this work. The amyloid-like nature of our synthetic tau K18 amyloid was further assessed by digestion with 10 µg/mL proteinase K, which resulted in a pattern of bands with lower molecular weight compared to the undigested sample. The relative resistance of protein aggregates to proteinase K digestion is another known feature of amyloids, and it appears to be correlated to the structural organization of the conformer and to the amount of β-sheet elements. The results we obtained are in line with previous works showing that recombinant tau aggregates are resistant to protease degradation (Iba *et al.* 2013; Falcon *et al.* 2015; Meyer *et al.* 2016), and therefore we concluded that our synthetic tau K18 fibrils can be considered as bona-fide amyloids.

Although recent work (Ghag *et al.* 2018) points at the sonicated synthetic aggregates as the species responsible for toxicity, we did not detect any significant effect after exposure to tau K18 amyloids. This discrepancy might be due to small differences in the preparations of the amyloids (isoform of tau, amount of heparin, shaking protocol, sonication procedure). For example, our sonicated fibrils are slightly smaller than the ones used in Ghag *et al.* (average height 4-6 nm), as they include also fragments with height ranging from 2 to 4 nm. As sonication randomly breaks long fibrils into smaller fragments, it might generate large variability between different preparations, and sometimes also among batches prepared in the same way. Indeed, as it can be observed from the graphs in Supplementary Fig. 3, we could detect mild cytotoxicity in all cell types with some batches of fibrils, even if it was not statistically significant. From the trend of the data, the slight reduction in cell viability appears to be correlated with the concentration of tau amyloids that was used. N2a *Prnp*$^{-/-}$ showed the strongest effect in terms of reduction of cell viability, and we think that this might be related to the increased sensitivity of cells lacking PrP^{C} to a wide range of insults (Brown et al. 1997; Brown et al. 2002).

We found that cells that express PrP^{C} on the cell surface (N2a) internalize more tau amyloids compared to the same cells from which the gene encoding PrP^{C} was removed (N2a *Prnp*$^{-/-}$). N2a *Prnp*$^{-/-}$ cells, even if deprived of PrP^{C}, were able to internalize a discrete number of fibrils, consistently with previous reports of multiple mechanisms occurring at the same time and independently from each other. However, when the prion protein was present, the number of internalized fibrils almost doubled, meaning that the PrP^{C}-mediated pathway contributed strongly to this process.

We performed a meta-analysis on published genomic and proteomic data to confirm the validity of our model and to exclude that the knock-down of PrP^{C} might in some way interfere with the expression of other tau receptors (Morozova *et al.* 2019; Rauch *et al.* 2018). Concerning N2a cell line, we found that specific tau receptors are poorly expressed. Indeed, expression of both HPSGs and muscarinic receptors M1 and M3 could not be detected, while low expression of

LRP1 has been reported (source: BioGPS Mouse Cell Type and Tissue Gene Expression Profiles). Nevertheless, as previously mentioned, tau amyloids have been shown to enter cells also through macropinocytosis and tunneling nanotubes, which might explain the results obtained in N2a *Prnp*$^{-/-}$. Concerning PrP knock-out cell lines, a proteomic study conducted in NMuMG cells (Mehrabian *et al.* 2014) only revealed the mild dysregulation of the HSPG syndecan-1 in knock-out cells compared the wild-type counterpart. However, this protein is typically expressed in epithelial and endothelial cells, therefore we deem it unlikely that it might play a relevant role in our neuroblastoma cell model. More recently, Macedo *et al.* conducted a proteomic study on wild-type and *Prnp*$^{-/-}$ PK1 neuroblastoma cell line to identify all differentially expressed proteins, with a specific focus on membrane proteins (Macedo *et al.* 2017). The analysis resulted in six differentially expressed proteins, none of which has ever been associated to the process of tau internalization. Hence, we could conclude that there is no evidence pointing towards an effect of *Prnp* ablation on the expression of other tau receptors.

The PrP^{C}-mediated internalization of tau k18 amyloids occurs most likely via endocytosis, since we observed an inhibition of the uptake upon lowering the temperature to 4°C. A similar effect occurred also with α-synuclein, suggesting that common energy-dependent mechanisms regulate the receptor-mediated internalization of different aggregated proteins (Reyes *et al.* 2019; Bieri *et al.* 2018; Desplats *et al.* 2009; Lee *et al.* 2008). The specific pathways regulating Aβ amyloids internalization are under debate, as endocytosis and passive diffusion were proposed to co-occur in the same neuron (Kandimalla *et al.* 2009). Nevertheless, the majority of data indicate a dynamin-dependent pathway, rather than clathrin-dependent, as the principal mechanism driving the internalization of α-synuclein and Aβ amyloids. Concerning tau, clathrin-mediated processes have been excluded in many different cell models, while the exact role of dynamin-dependent endocytosis is still unclear (Holmes *et al.* 2013; Demaegd *et al.* 2018; Evans *et al.* 2018). Although in one case the inhibition of dynamin did not result in decreased uptake (Holmes *et al.* 2013), other works showed that treatments with the drug Dynasore reduced the internalization of tau aggregates. Moreover, the inhibition of Bin1 protein, which interacts with clathrin and recruits dynamin in a mixed pathway, led to an impairment of the entrance of tau aggregates composed only of the microtubule-binding domains (Calafate *et al.* 2016). Therefore, we speculate that dynamin might be involved in the energy-dependent mechanism of PrP^{C}-mediated uptake in our cell model.

The role of PrP^{C} was orthogonally confirmed by the observation that the targeting of the N-terminus or the hydrophobic domain of PrP^{C} using antibodies lead to a reduction of the internalized fibrils. Most intriguingly, we discovered that the interaction between PrP^{C} and tau fibrils has mutual effects on both partners; while the former acts as a receptor, the presence of

tau aggregates leads to an increase of the cellular level of the prion protein, which is re-localized mainly on the plasma membrane where it could perform its receptor activity. The increase in PrP^C could be due either to the trafficking of the newly synthesized PrP^C on the surface, or to a longer retention on the membrane as a consequence of the interaction with the fibrils, as no changes in *Prnp* expression levels were detected. Given that the prion protein facilitates the internalization of tau amyloids, we hypothesize that a higher amount of PrP^C exposed outside the cells might result in more extracellular tau fibrils gaining cell entrance Although this phenomenon might be a simple side-effect of the interaction and subsequent internalization of the aggregates, we deem it likely that tau fibrils are boosting their own spreading by increasing the number of receptor molecules on the cell surface. A similar hypothesis has been proved true in the case of intercellular transfer of tau amyloids through tunneling nanotubes, where extracellular tau species (monomers and fibrils) activated the formation of new nanotubes and therefore facilitated fibrillar tau transport between neurons (Tardivel *et al.* 2016). On the other hand, protein aggregates (tau and synuclein) are trafficked in early endosomes and lysosomes after the internalization (Evans *et al.* 2018; Masaracchia *et al.* 2018; Aulic *et al.* 2017). The need of the cell to deal quickly with a large amount of exogenous and potentially dangerous material might clog the degradation system, with subsequent impact on the normal turnover of the endogenous proteins. Indeed, a similar effect on PrP levels has been reported after treatment with synuclein fibrils (Aulic *et al.* 2017), although the localization of the excess protein was not investigated. Alternatively, the binding of the amyloids to PrP^C on the cell membrane might simply impede its internalization and retain the protein in its position, therefore leading to a general increase as the newly synthesized protein follows its normal pathway all the way up to the surface.

Together with the previously mentioned electrophysiological data (Ondrejcak *et al.* 2018; Ondrejcak *et al.* 2019), our observations on the mechanicistic role of PrP^C in the spreading of tau pathology provide a more comprehensive outlook on the progression of tauopathies. Moreover, this work gives additional strong and orthogonal evidence to the therapeutic potential of anti-PrP antibodies in the treatment of tauopathies.

We observed that the scrapie load in cell cultures decreased after incubation with tau K18 fibrils. Tau-mediated clearance was independent of the PrP^{Sc} conformation, as a similar reduction was observed for both RML and 22L prion strains. One way in which tau K18 amyloids might lead to PrP^{Sc} reduction is through a direct binding to either PrP^C or PrP^{Sc}, inhibiting prion conversion by depleting respectively the pool of the substrate or of the template. Indeed, tau K18 fibrils bind to PrP^C and promote its processing into the N1 and C1 fragments, which reduces the amount of cellular prion protein available for the conversion. The similar effects observed after the exposure of two different prion strains to tau aggregates seems to suggest that PrP^{Sc} might not be the

target. As the exact structure of PrP^{Sc} is undefined, the structural differences distinguishing the RML and 22L prion strains are not known, and could be so subtle not to impact the binding of K18 fibrils in a detectable manner. In view of the wealth of data suggesting that PrP^{C} interacts with many amyloids, the most parsimonious interpretation is that tau K18 amyloids interacts with the PrP^{C}.

Our findings are likely to have a deep impact on the explanation of the co-presence of tau and PrP deposits found in some cases of prion diseases. Specifically, in some patients the prion protein burden was found to be correlated with the presence of tau aggregates in the forms of rods and stubs (Reiniger *et al.* 2011), and dystrophic neurites positive for anti-phospho tau antibodies were found to colocalize with prion plaques in cases of sCJD, vCJD and GSS (Giaccone *et al.* 2008; Sikorska *et al.* 2009). While the co-deposition of NFTs and prion plaques is considered as a sort of side-effect in classical prion disorders, it becomes the major sign of a rare form of prion disorder called PrP-cerebral amyloid angiopathy (PrP-CAA) (Ghetti et al. 1996). This peculiar case of dementia arises from a nonsense mutation at codon 145 of PrP, and is characterised by extended PrP deposition in the walls of small and medium-size vessels, as well as in the surrounding parenchyma. Neurofibrillary tangles and neurophil threads are abundant especially in the pyramidal and granule cells of the hippocampus, and are closely associated with parenchymal amyloid plaques. However, the relationship between prion and tau pathologies remain elusive. In view of our data, we think that the presence of both protein deposits might not be a pure coincidence. While it has been proposed that PrP deposits might in some cases trigger tau phosphorylation, our observations suggest that also tau amyloids could influence the fate of PrP aggregates. As already discussed for the cases of the co-deposition of PrP and synuclein (Aulic *et al.* 2017), we believe that deeper investigations on these cases (i.e. duration of the disease course, severity of the symptoms) might open new possible interpretation of this phenomenon.

In conclusion, here we provide evidence of another relevant role for PrP^{C} in mediating the internalization of exogenous tau fibrils, therefore contributing to the cell-to-cell spreading of tau K18 amyloids and to the onset of the pathology. The interaction between tau fibrils and the cellular prion protein seems to affect also the process of prion replication in prion-infected cell lines. This occurs probably through the inhibition of the mechanism of PrP^{C} conversion into PrP^{Sc}, due to an increased rate of α-cleavage of PrP^{C} stimulated by the binding to tau fibrils.

Involves human subjects:

If yes: Informed consent & ethics approval achieved:

=> if yes, please ensure that the info "Informed consent was achieved for all subjects, and the experiments were approved by the local ethics committee." is included in the Methods.

ARRIVE guidelines have been followed:

Yes

=> if it is a Review or Editorial, skip complete sentence => if No, include a statement in the "Conflict of interest disclosure" section: "ARRIVE guidelines were not followed for the following reason:

"

(edit phrasing to form a complete sentence as necessary).

=> if Yes, insert in the "Conflict of interest disclosure" section:

"All experiments were conducted in compliance with the ARRIVE guidelines." unless it is a Review or Editorial

Conflicts of interest: none

=> if 'none', insert "The authors have no conflict of interest to declare."

=> otherwise insert info unless it is already included

Acknowledgements

Funding was provided by JPND Reframe Consortium to G.L.

Preprint on BioRxiv: https://www.biorxiv.org/content/10.1101/2020.01.19.911644v1.

E.D.C. would like to acknowledge Fabio Perissinotto, PhD, for the AFM analysis of tau K18 amyloids, Rabah Soliymani, PhD, for Mass Spectrometry analysis, Camila Gherardelli for help and support with the experiments of tau amyloids internalization, and Asvin Lakkaraju, PhD, for help in setting up some of the protocols.

Conflict of interest: The authors declare that they have no conflict of interest with the contest of this article.

Author contributions: E.D.C. conceived and performed the experiments, wrote the manuscript. L.C. Performed experiments of PrP^{Sc} clearance by tau K18 amyloids. S.V. Performed pull-down experiments. M.G. Support with microscopy images acquisition and analysis. E.B. and F.M. Performed TEM analysis. A.A. Suggested experiments and revised the paper. G.L. Conceived and designed the experiments.

References

Abe, M. and Bonini, N. M. (2013) MicroRNAs and neurodegeneration: role and impact. *Trends Cell Biol* **23,** 30-36.

Aguzzi, A. (2009) Cell biology: Beyond the prion principle. *Nature* **459,** 924-925.

Aulic, S., Le, T. T., Moda, F. et al. (2014) Defined alpha-synuclein prion-like molecular assemblies spreading in cell culture. *BMC Neurosci* **15,** 69.

Aulic, S., Masperone, L., Narkiewicz, J. et al. (2017) alpha-Synuclein Amyloids Hijack Prion Protein to Gain Cell Entry, Facilitate Cell-to-Cell Spreading and Block Prion Replication. *Scientific reports* **7,** 10050.

Barghorn, S., Biernat, J. and Mandelkow, E. (2005) Purification of recombinant tau protein and preparation of Alzheimer-paired helical filaments in vitro. *Methods Mol Biol* **299,** 35-51.

Bieri, G., Gitler, A. D. and Brahic, M. (2018) Internalization, axonal transport and release of fibrillar forms of alpha-synuclein. *Neurobiology of disease* **109,** 219-225.

Boucrot, E. and Kirchhausen, T. (2008) Mammalian cells change volume during mitosis. *PloS one* **3,** e1477.

Braak, H. and Braak, E. (1991) Neuropathological stageing of Alzheimer-related changes. *Acta neuropathologica* **82,** 239-259.

Butler, D. A., Scott, M. R., Bockman, J. M., Borchelt, D. R., Taraboulos, A., Hsiao, K. K., Kingsbury, D. T. and Prusiner, S. B. (1988) Scrapie-infected murine neuroblastoma cells produce protease-resistant prion proteins. *J Virol* **62,** 1558-1564.

Calafate, S., Flavin, W., Verstreken, P. and Moechars, D. (2016) Loss of Bin1 Promotes the Propagation of Tau Pathology. *Cell Rep* **17,** 931-940.

Calella, A. M., Farinelli, M., Nuvolone, M., Mirante, O., Moos, R., Falsig, J., Mansuy, I. M. and Aguzzi, A. (2010) Prion protein and Abeta-related synaptic toxicity impairment. *EMBO Mol Med* **2,** 306-314.

Chen, S., Yadav, S. P. and Surewicz, W. K. (2010) Interaction between human prion protein and amyloid-beta (Abeta) oligomers: role OF N-terminal residues. *The Journal of biological chemistry* **285,** 26377-26383.

Clavaguera, F., Akatsu, H., Fraser, G. et al. (2013) Brain homogenates from human tauopathies induce tau inclusions in mouse brain. *Proceedings of the National Academy of Sciences of the United States of America* **110,** 9535-9540.

Clavaguera, F., Bolmont, T., Crowther, R. A. et al. (2009) Transmission and spreading of tauopathy in transgenic mouse brain. *Nat Cell Biol* **11,** 909-913.

De Cecco, E. and Legname, G. (2018) The role of the prion protein in the internalization of alpha-synuclein amyloids. *Prion* **12,** 23-27.

Demaegd, K., Schymkowitz, J. and Rousseau, F. (2018) Transcellular Spreading of Tau in Tauopathies. *Chembiochem* **19,** 2424-2432.

Desplats, P., Lee, H. J., Bae, E. J., Patrick, C., Rockenstein, E., Crews, L., Spencer, B., Masliah, E. and Lee, S. J. (2009) Inclusion formation and neuronal cell death through neuron-to-neuron transmission of alpha-synuclein. *Proceedings of the National Academy of Sciences of the United States of America* **106,** 13010-13015.

Evans, L. D., Wassmer, T., Fraser, G., Smith, J., Perkinton, M., Billinton, A. and Livesey, F. J. (2018) Extracellular Monomeric and Aggregated Tau Efficiently Enter Human Neurons through Overlapping but Distinct Pathways. *Cell Rep* **22,** 3612-3624.

Falcon, B., Cavallini, A., Angers, R. et al. (2015) Conformation determines the seeding potencies of native and recombinant Tau aggregates. *The Journal of biological chemistry* **290,** 1049-1065.

Ferreira, D. G., Temido-Ferreira, M., Miranda, H. V. et al. (2017) alpha-synuclein interacts with PrPC to induce cognitive impairment through mGluR5 and NMDAR2B. *Nature neuroscience* **20,** 1569-1579.

Fluharty, B. R., Biasini, E., Stravalaci, M. et al. (2013) An N-terminal fragment of the prion protein binds to amyloid-beta oligomers and inhibits their neurotoxicity in vivo. *The Journal of biological chemistry* **288,** 7857-7866.

Frost, B., Ollesch, J., Wille, H. and Diamond, M. I. (2009) Conformational diversity of wild-type Tau fibrils specified by templated conformation change. *The Journal of biological chemistry* **284,** 3546-3551.

Ghag, G., Bhatt, N., Cantu, D. V., Guerrero-Munoz, M. J., Ellsworth, A., Sengupta, U. and Kayed, R. (2018) Soluble tau aggregates, not large fibrils, are the toxic species that display seeding and cross-seeding behavior. *Protein Science* **27,** 1901-1909.

Ghetti, B., Piccardo, P., Spillantini, M. G. et al. (1996) Vascular variant of prion protein cerebral amyloidosis with tau-positive neurofibrillary tangles: the phenotype of the stop codon 145 mutation in PRNP. *Proceedings of the National Academy of Sciences of the United States of America* **93,** 744-748.

Giaccone, G., Mangieri, M., Capobianco, R., Limido, L., Hauw, J. J., Haik, S., Fociani, P., Bugiani, O. and Tagliavini, F. (2008) Tauopathy in human and experimental variant Creutzfeldt-Jakob disease. *Neurobiology of aging* **29,** 1864-1873.

Goniotaki, D., Lakkaraju, A. K. K., Shrivastava, A. N. et al. (2017) Inhibition of group-I metabotropic glutamate receptors protects against prion toxicity. *PLoS Pathog* **13,** e1006733.

Guo, J. L. and Lee, V. M. (2011) Seeding of normal Tau by pathological Tau conformers drives pathogenesis of Alzheimer-like tangles. *The Journal of biological chemistry* **286,** 15317-15331.

Han, J., Zhang, J., Yao, H. et al. (2006) Study on interaction between microtubule associated protein tau and prion protein. *Sci China C Life Sci* **49,** 473-479.

Holmes, B. B., DeVos, S. L., Kfoury, N. et al. (2013) Heparan sulfate proteoglycans mediate internalization and propagation of specific proteopathic seeds. *Proceedings of the National Academy of Sciences of the United States of America* **110,** E3138-3147.

Holmes, B. B., Furman, J. L., Mahan, T. E. et al. (2014) Proteopathic tau seeding predicts tauopathy in vivo. *Proceedings of the National Academy of Sciences of the United States of America* **111,** E4376-4385.

Iba, M., Guo, J. L., McBride, J. D., Zhang, B., Trojanowski, J. Q. and Lee, V. M. (2013) Synthetic tau fibrils mediate transmission of neurofibrillary tangles in a transgenic mouse model of Alzheimer's-like tauopathy. *The Journal of neuroscience : the official journal of the Society for Neuroscience* **33,** 1024-1037.

Iba, M., McBride, J. D., Guo, J. L., Zhang, B., Trojanowski, J. Q. and Lee, V. M. (2015) Tau pathology spread in PS19 tau transgenic mice following locus coeruleus (LC) injections of synthetic tau fibrils is determined by the LC's afferent and efferent connections. *Acta neuropathologica* **130,** 349-362.

Kandimalla, K. K., Scott, O. G., Fulzele, S., Davidson, M. W. and Poduslo, J. F. (2009) Mechanism of neuronal versus endothelial cell uptake of Alzheimer's disease amyloid beta protein. *PloS one* **4,** e4627.

Karpowicz, R. J., Jr., Haney, C. M., Mihaila, T. S., Sandler, R. M., Petersson, E. J. and Lee, V. M. (2017) Selective imaging of internalized proteopathic alpha-synuclein seeds in primary neurons reveals mechanistic insight into transmission of synucleinopathies. *The Journal of biological chemistry* **292,** 13482-13497.

Kessels, H. W., Nguyen, L. N., Nabavi, S. and Malinow, R. (2010) The prion protein as a receptor for amyloid-beta. *Nature* **466,** E3-4; discussion E4-5.

Khlistunova, I., Biernat, J., Wang, Y., Pickhardt, M., von Bergen, M., Gazova, Z., Mandelkow, E. and Mandelkow, E. M. (2006) Inducible expression of Tau repeat domain in cell models of tauopathy: aggregation is toxic to cells but can be reversed by inhibitor drugs. *The Journal of biological chemistry* **281,** 1205-1214.

La Vitola, P., Beeg, M., Balducci, C. et al. (2019) Cellular prion protein neither binds to alpha-synuclein oligomers nor mediates their detrimental effects. *Brain* **142,** 249-254.

Lee, H. J., Suk, J. E., Bae, E. J., Lee, J. H., Paik, S. R. and Lee, S. J. (2008) Assembly-dependent endocytosis and clearance of extracellular alpha-synuclein. *The international journal of biochemistry & cell biology* **40,** 1835-1849.

Macedo, J. A., Schrama, D., Duarte, I., Tavares, E., Renaut, J., Futschik, M. E., Rodrigues, P. M. and Melo, E. P. (2017) Membrane-enriched proteome changes and prion protein expression during neural differentiation and in neuroblastoma cells. *BMC Genomics* **18,** 319.

Masaracchia, C., Hnida, M., Gerhardt, E. et al. (2018) Membrane binding, internalization, and sorting of alpha-synuclein in the cell. *Acta neuropathologica communications* **6,** 79.

Mehrabian, M., Brethour, D., MacIsaac, S., Kim, J. K., Gunawardana, C. G., Wang, H. and Schmitt-Ulms, G. (2014) CRISPR-Cas9-based knockout of the prion protein and its effect on the proteome. *PloS one* **9,** e114594.

Meyer, V., Holden, M. R., Weismiller, H. A., Eaton, G. R., Eaton, S. S. and Margittai, M. (2016) Fracture and Growth Are Competing Forces Determining the Fate of Conformers in Tau Fibril Populations. *The Journal of biological chemistry* **291,** 12271-12281.

Mirbaha, H., Holmes, B. B., Sanders, D. W., Bieschke, J. and Diamond, M. I. (2015) Tau Trimers Are the Minimal Propagation Unit Spontaneously Internalized to Seed Intracellular Aggregation. *The Journal of biological chemistry* **290,** 14893-14903.

Morozova, V., Cohen, L. S., Makki, A. E., Shur, A., Pilar, G., El Idrissi, A. and Alonso, A. D. (2019) Normal and Pathological Tau Uptake Mediated by M1/M3 Muscarinic Receptors Promotes Opposite Neuronal Changes. *Front Cell Neurosci* **13,** 403.

Ondrejcak, T., Hu, N. W., Qi, Y. et al. (2019) Soluble tau aggregates inhibit synaptic long-term depression and amyloid beta-facilitated LTD in vivo. *Neurobiology of disease* **127,** 582-590.

Ondrejcak, T., Klyubin, I., Corbett, G. T. et al. (2018) Cellular Prion Protein Mediates the Disruption of Hippocampal Synaptic Plasticity by Soluble Tau In Vivo. *The Journal of neuroscience : the official journal of the Society for Neuroscience* **38,** 10595-10606.

Piccardo, P., King, D., Brown, D. and Barron, R. M. (2017) Variable tau accumulation in murine models with abnormal prion protein deposits. *J Neurol Sci* **383,** 142-150.

Polymenidou, M., Moos, R., Scott, M. et al. (2008) The POM monoclonals: a comprehensive set of antibodies to non-overlapping prion protein epitopes. *PloS one* **3,** e3872.

Rauch, J. N., Chen, J. J., Sorum, A. W., Miller, G. M., Sharf, T., See, S. K., Hsieh-Wilson, L. C., Kampmann, M. and Kosik, K. S. (2018) Tau Internalization is Regulated by 6-O Sulfation on Heparan Sulfate Proteoglycans (HSPGs). *Scientific reports* **8,** 6382.

Reiniger, L., Lukic, A., Linehan, J., Rudge, P., Collinge, J., Mead, S. and Brandner, S. (2011) Tau, prions and Abeta: the triad of neurodegeneration. *Acta neuropathologica* **121,** 5-20.

Resenberger, U. K., Harmeier, A., Woerner, A. C. et al. (2011) The cellular prion protein mediates neurotoxic signalling of beta-sheet-rich conformers independent of prion replication. *The EMBO journal* **30,** 2057-2070.

Resenberger, U. K., Winklhofer, K. F. and Tatzelt, J. (2012) Cellular prion protein mediates toxic signaling of amyloid beta. *Neurodegener Dis* **10,** 298-300.

Reyes, J. F., Sackmann, C., Hoffmann, A., Svenningsson, P., Winkler, J., Ingelsson, M. and Hallbeck, M. (2019) Binding of α-synuclein oligomers to Cx32 facilitates protein uptake and transfer in neurons and oligodendrocytes. *Acta neuropathologica* **138,** 23-47.

Rossi, M., Kai, H., Baiardi, S., Bartoletti-Stella, A., Carlà, B., Zenesini, C., Capellari, S., Kitamoto, T. and Parchi, P. (2019) The characterization of AD/PART co-pathology in CJD suggests independent pathogenic mechanisms and no cross-seeding between misfolded Aβ and prion proteins. *Acta neuropathologica communications* **7,** 53.

Sanders, D. W., Kaufman, S. K., DeVos, S. L. et al. (2014) Distinct tau prion strains propagate in cells and mice and define different tauopathies. *Neuron* **82,** 1271-1288.

Sikorska, B., Liberski, P. P., Sobow, T., Budka, H. and Ironside, J. W. (2009) Ultrastructural study of florid plaques in variant Creutzfeldt-Jakob disease: a comparison with amyloid plaques

in kuru, sporadic Creutzfeldt-Jakob disease and Gerstmann-Straussler-Scheinker disease. *Neuropathol Appl Neurobiol* **35,** 46-59.

Stincardini, C., Massignan, T., Biggi, S. et al. (2017) An antipsychotic drug exerts anti-prion effects by altering the localization of the cellular prion protein. *PloS one* **12,** e0182589.

Tardivel, M., Begard, S., Bousset, L., Dujardin, S., Coens, A., Melki, R., Buee, L. and Colin, M. (2016) Tunneling nanotube (TNT)-mediated neuron-to neuron transfer of pathological Tau protein assemblies. *Acta neuropathologica communications* **4,** 117.

Um, J. W., Nygaard, H. B., Heiss, J. K., Kostylev, M. A., Stagi, M., Vortmeyer, A., Wisniewski, T., Gunther, E. C. and Strittmatter, S. M. (2012) Alzheimer amyloid-beta oligomer bound to postsynaptic prion protein activates Fyn to impair neurons. *Nature neuroscience* **15,** 1227-1235.

Urrea, L., Segura-Feliu, M., Masuda-Suzukake, M. et al. (2017) Involvement of Cellular Prion Protein in alpha-Synuclein Transport in Neurons. *Molecular neurobiology*.

Wu, J. W., Herman, M., Liu, L. et al. (2013) Small misfolded Tau species are internalized via bulk endocytosis and anterogradely and retrogradely transported in neurons. *The Journal of biological chemistry* **288,** 1856-1870.

Zhang, Y., Hashemi, M., Lv, Z., Williams, B., Popov, K. I., Dokholyan, N. V. and Lyubchenko, Y. L. (2018) High-speed atomic force microscopy reveals structural dynamics of alpha-synuclein monomers and dimers. *J Chem Phys* **148,** 123322.

REAGENT or RESOURCE	SOURCE	IDENTIFIER
Antibodies		
Monoclonal mouse anti-beta actin, HRP-conjugated	SIGMA	Cat #A3854 RRID:AB_262011
HRP conjugated goat anti-mouse antibody	Jackson laboratories	Cat #115-035-003 RRID:AB_10015289
mouse anti-tau RD4 antibody	Millipore	Cat #05-804 RRID:AB_310014
AlexaFluor 594 conjugated goat anti-mouse antibody	ThermoFisher	Cat #A-11032 RRID:AB_2534091
Human anti-PrP antibody D18	Dr. Stanley Prusiner (UCSF)	N/A
Mouse anti-PrP antibody W226		
Bacterial and Virus Strains		
BL21(DE3) E.coli bacterial strain	New England Biolabs	Cat #C2527H
Chemicals, kits and other equipment		
HiTrap SP FF columns	Sigma/Merck	Cat #GE17-5054-01
HiLoad® 26/600 Superdex® 200 pg	Sigma/Merck	Cat #GE28-9893-36
AlexaFluor 488 succinimidyl ester	ThermoFisher	Cat #A20000
HCS Cell Mask Blue Stain	ThermoFisher	Cat #H32720
Heparin sodium salt	Sigma	Cat #H3149
3 mm glass beads	Sigma	Cat #1040150500
LysoTracker Red DND-2 dye	ThermoFisher	Cat #L7528
Complete™ ULTRA Tablets, EDTA-free, glass vials Protease Inhibitor Cocktail	Sigma	Cat #5892953001
Pierce BCA Protein Assay kit	ThermoFisher	Cat #23225
NeutrAvidin Agarose Resins	ThermoFisher	Cat #29200
Trypan Blue Solution	Sigma	Cat #T8154

Fluoromount-G	ThermoFisher	Cat #00-4958-02
Immobilon PVDF membranes	Millipore	Cat #IPVH00010
PureLink RNA MiniKit with TRIzol® Reagent	ThermoFisher	Cat #12183018A
PureLink DNAse Set	Thermofisher	Cat #12185010
iQ™ SYBR® Green Supermix	Bio-Rad	Cat #170-8882
PNGaseF	New England Biolabs	Cat #P0704L
Geneticin (G418)	ThermoFisher Scientific	Cat #10131035
Opti-MEM reduced serum medium without phenol	ThermoFisher Scientific	Cat #11058-21
Minimum Essential Medium (MEM)	GIBCO	Cat #32561029
Penicillin-streptomycin (PenStrep)	ThermoFisher Scientific	Cat #25300-054
Fetal Bovine Serum (FBS)	Cat# SV30160.03HI	GE Healthcare Bio-Sciences Austria GmbH
Phosphate buffered saline (PBS) without Ca2+ and Mg2+	ThermoFisher Scientific	Cat #14190-250
PDL (Poly-D-lysine hydrobromide, average mol wt 30,000-70,000)	ThermoFisher Scientific	Cat # P7280-5mg
Immobilon Classico Western HRP Substrate	Merck	#WBLUC0500
Dimethyl sulfoxide (DMSO)	Sigma	#D8418-50ML
Experimental Models: Cell Lines		
Neuro-2a cell line	ATCC	N/A
Neuro-2a, *Prnp*$^{-/-}$	Dr. Gerold Schmitt-Ulms (Mehrabian et al., 2014)	N/A
Scrapie Neuro-2a, RML infected	Dr. Stanley Prusiner (Butler et al., 1988)	N/A
Scrapie Neuro-2a, 22L infected	Karolinska Institute	N/A
Oligonucleotides		

Forward primer targeting the *Prnp* transcript for qPCR: GAGACCGATGTGAAGATGATGGA	This paper	N/A
Reverse primer targeting the *Prnp* transcript for qPCR: TAATAGGCCTGGGACTCCTTCTG	This paper	N/A
GAPDH housekeeping gene forward primer for qPCR: CCTGCACCACCAACTGCTTA	This paper	N/A
GAPDH housekeeping gene reverse primer for qPCR: CTGTCACCTTCACCGTTCC	This paper	N/A
Recombinant DNA		
pET-11a:tauK18	Genscript	N/A
pcDNA3.1-Mouse Prp Full-length	Aulic et al., 2014	N/A
Software and Algorithms		
Fiji	https://fiji.sc	N/A
NIS Elements and NIS Elements Viewer	https://www.nikon.com/products/microscope-solutions/lineup/img_soft/nis-elements/	N/A
GraphPad Prism software (version 7.0a)	https://www.graphpad.com/scientific-software/prism/	RRID: SCR_002798
Volocity Workstation (version 4.1)	PerkinElmer	N/A
Uvitec Alliance	https://www.uvitec.co.uk/it/uvitec-it/	N/A

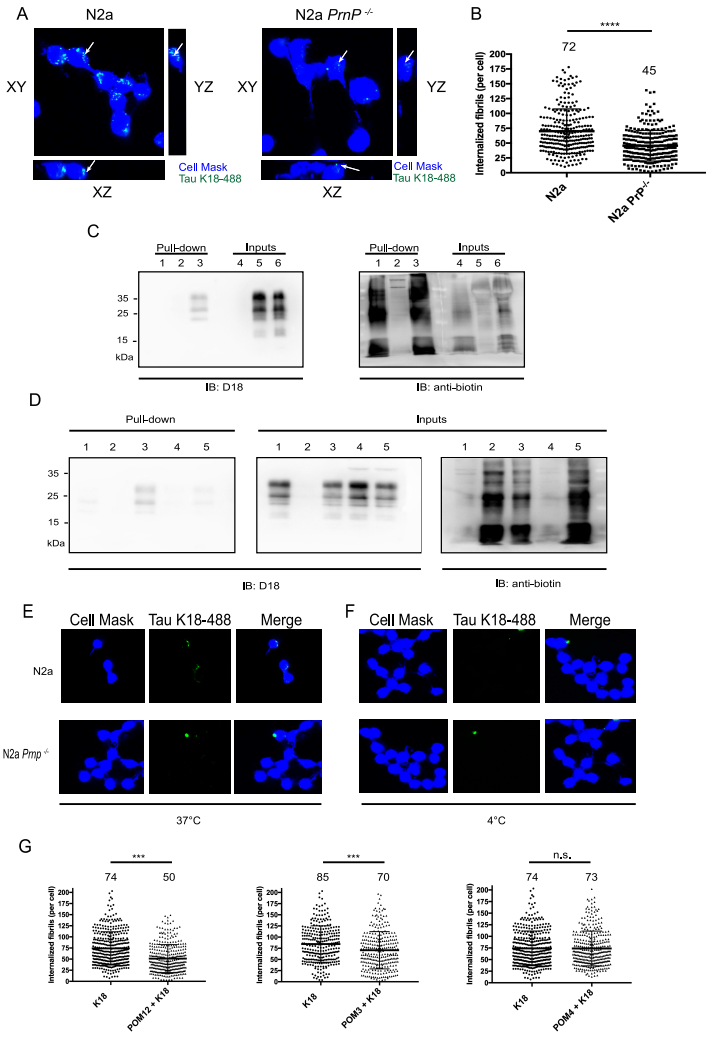

Figure 1. Uptake of tau K18 amyloids in mouse neuroblastoma cell lines. (A) Confocal microscopy images showing the orthogonal views of the central section of the 3D Z-stack for N2a and N2a *Prnp*$^{-/-}$ (in blue) treated with tau K18 fibrils (in green) for 24 hours. (B) Scatter plot showing the distribution of the number of internalized fibrils in N2a and N2a *Prnp*$^{-/-}$ cells. A total of three hundred cells were counted in blind in three independent experiments. Numbers on top indicate the average number of internalized fibrils. Data were evaluated with unpaired T-test with Welch's correction. Statistical analysis is indicated as: * = p <0.05, ** = p< 0.01, *** = p<0.001, **** = p<0.0001.. (C) Western Blot of pulled down samples (lanes 1-3) and input samples (lanes 4-6). Lane 1: K18 fibrils only; lane 2: N2a lysate only; lane 3: K18 fibrils and cell lysate. Lane 4: K18 fibrils only; lane 5: N2a cell lysate only; lane 6: K18 fibrils and cell lysate. The membrane was probed

with human anti-PrP^C antibody D18 and with anti-biotin to visualize tau K18 amyloids. (D) Western Blot of pulled down samples and input samples. Lane 1: N2a lysate only; lane 2: K18 fibrils only; lane 3: K18 fibrils and cell lysate. Lane 4: N2a cell lysate + POM12; lane 5: N2a cell lysate + POM12 + tau K18 amyloids. The membrane was probed with human anti-PrP^C antibody D18 and with anti-biotin to visualize tau K18. (E) and (F) Internalization of tau K18 amyloids by N2a and *N2a Prnp*$^{-/-}$ cells at 37°C (E) and 4°C (F). Images were acquired using a confocal microscope as series of Z-stacks and the analysis was carried out in 3D. Images show one of the central sections of the stack, both as separate channels and as a merge of the two channels. (G) Scatter plots representing the distribution of internalized fibrils in N2a cells treated only with tau K18 fibrils and in N2a that were pre-treated with different anti-PrP^C antibodies. Numbers on top indicate the average number of internalized fibrils. Data were evaluated with unpaired T-test with Welch's correction. Statistical analysis is indicated as: *= $p<0.05$; **= $p<0.01$; ***= $p<0.001$.

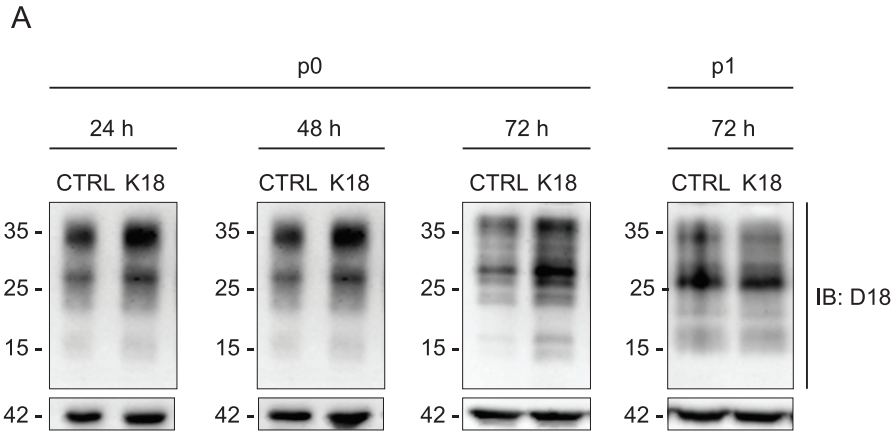

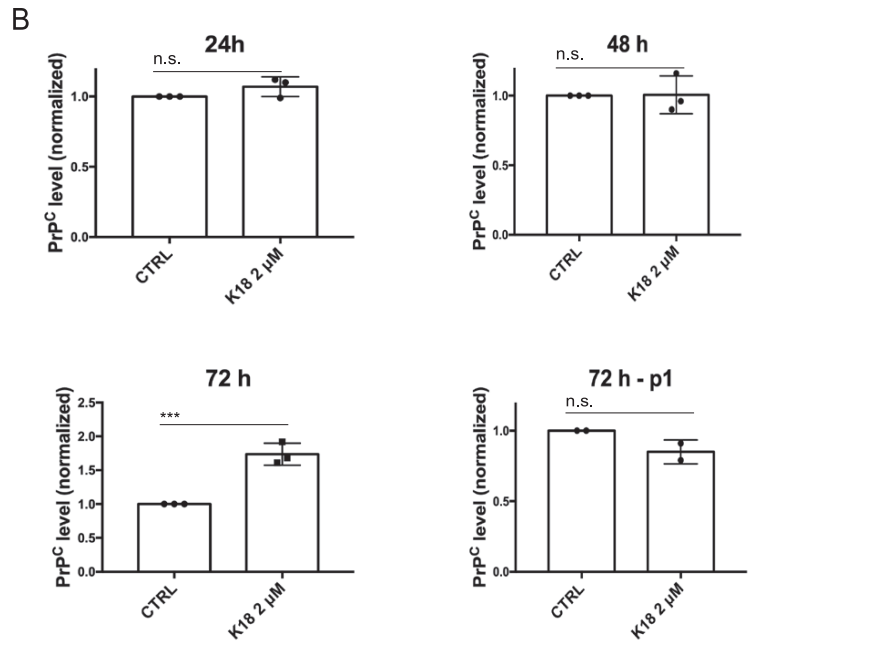

Figure 2. Exposure of N2a cells to tau K18 fibrils induces an increase of the endogenous prion protein. (A) Western blot analysis of N2a cells treated with 2 µM of tau K18 fibrils for 24, 48 and 72 hours and of the first passage of N2a treated for 72 hours. Membranes were probed with human anti-PrP antibody D18. (B) Quantification of three independent experiments. Data are represented as the percentage of total PrP relative to ß-actin. ß-actin is a loading control. Data are represented as mean ± SD. Data were evaluated by unpaired T-test. Statistical analysis is indicated as: n.s.= not significant; *= $p<0.05$; **= $p<0.01$; ***= $p<0.001$.

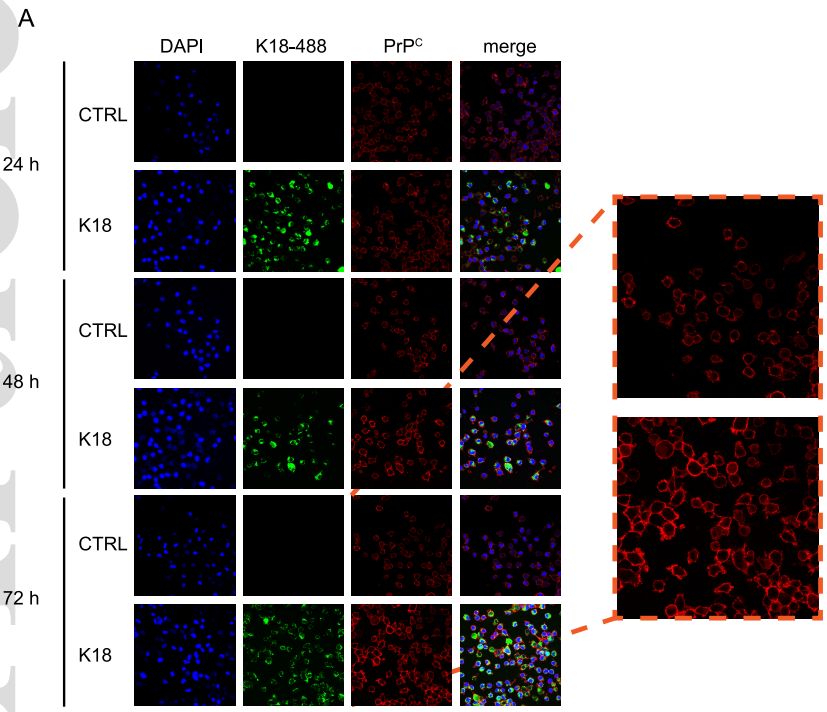

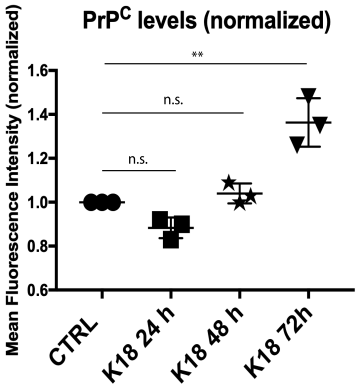

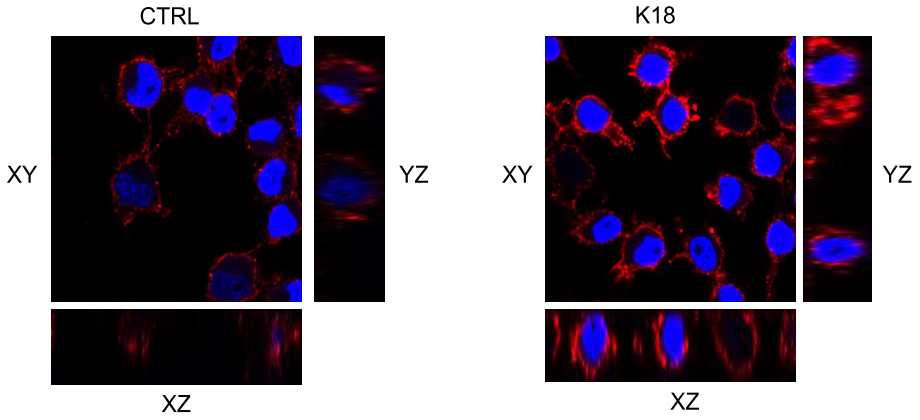

Figure 3. Exposure of N2a cells to tau K18 fibrils induces an increase of the endogenous prion protein. (A) Representative immunofluorescence images of untreated and treated N2a at three different timepoints. Membrane staining for PrP^C was performed at 4°C on alive cells using the W226 antibody. The magnified sections show a visible difference in the fluorescence intensity associated to PrP^C between control cells and cells treated for 72 hours. In all the images, the green signal corresponds to Tau K18 amyloids and the red signal to PrP^C. (B) Scatter plot of the intensity of the PrP-associated membrane staining of treated N2a compared to control cells. The intensity values, which correlates with the levels of PrP on the membrane, is reported as the ratio between the average intensities of treated and control cells for each timepoint. Controls have been normalized to 1. The three values represent three independent experiments, in which 700 cells for each condition were analysed. Data have been evaluated with unpaired T-test. Statistical analysis is indicated as: n.s.= not significant; *= $p<0.05$; **= $p<0.01$; ***= $p<0.001$. (C) Orthogonal views of the central section of the 3D Z-stack for N2a control cells and N2a treated with K18 amyloids for 72 hours.

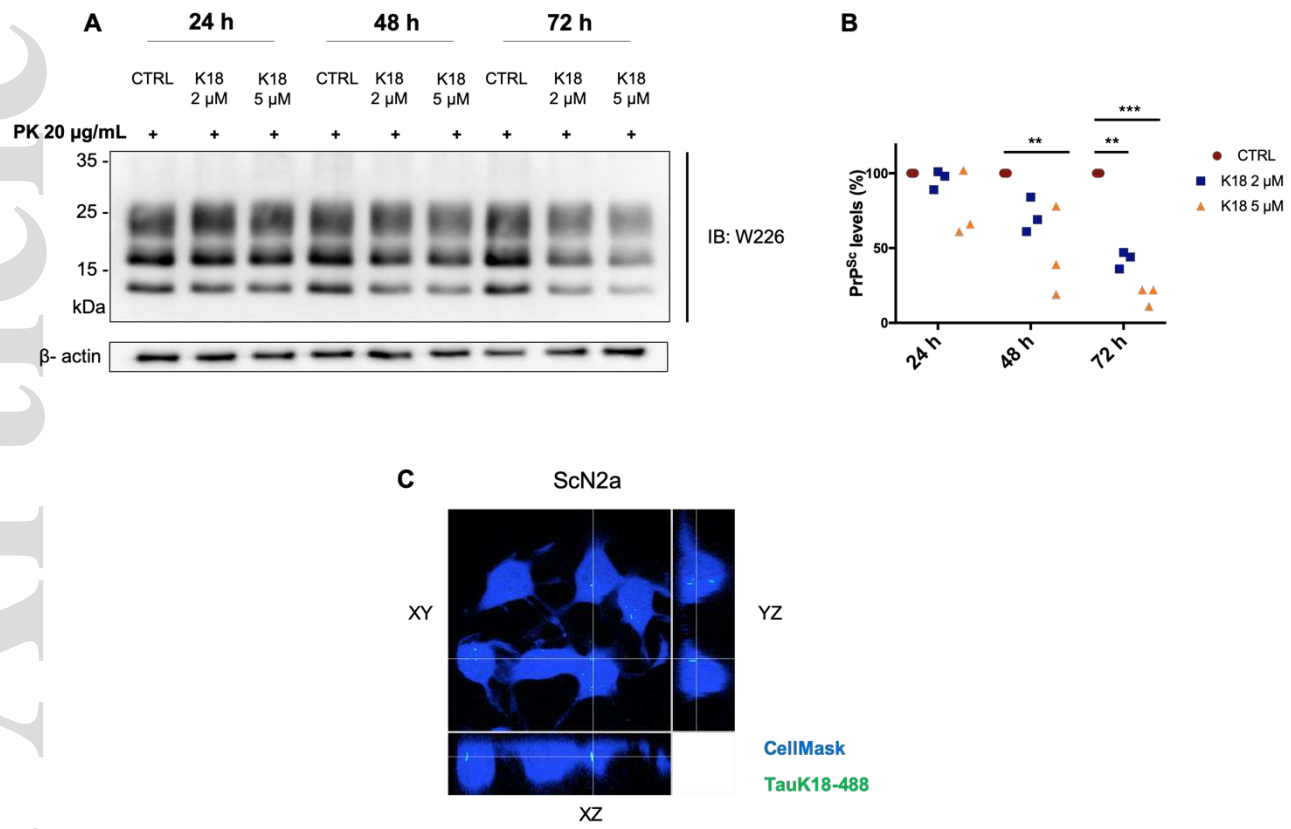

Figure 4. Tau-induced PrP^{Sc} clearance in ScN2a RML cell line at different timepoints. (A) Western Blot analysis of PK-resistant PrP^{Sc} upon treatment with different concentrations of tau K18 amyloids at 24 hours, 48 hours and 72 hours. (B) Quantification of three independent experiments. Values are shown as a percentage of PK-resistant form relative to β-actin. β-Actin is a loading control. Data are represented as mean ± SD. Data were evaluated by one-way ANOVA with multiple comparisons. Statistical analysis is indicated as: *= $p < 0.05$, **= $p < 0.01$, ***= $p < 0.001$. (C) Confocal microscopy image showing the orthogonal views of the central section of the 3D Z-stack of ScN2a RML cells treated with 2 µM of tau K18 amyloids (in green) for 72 hours.

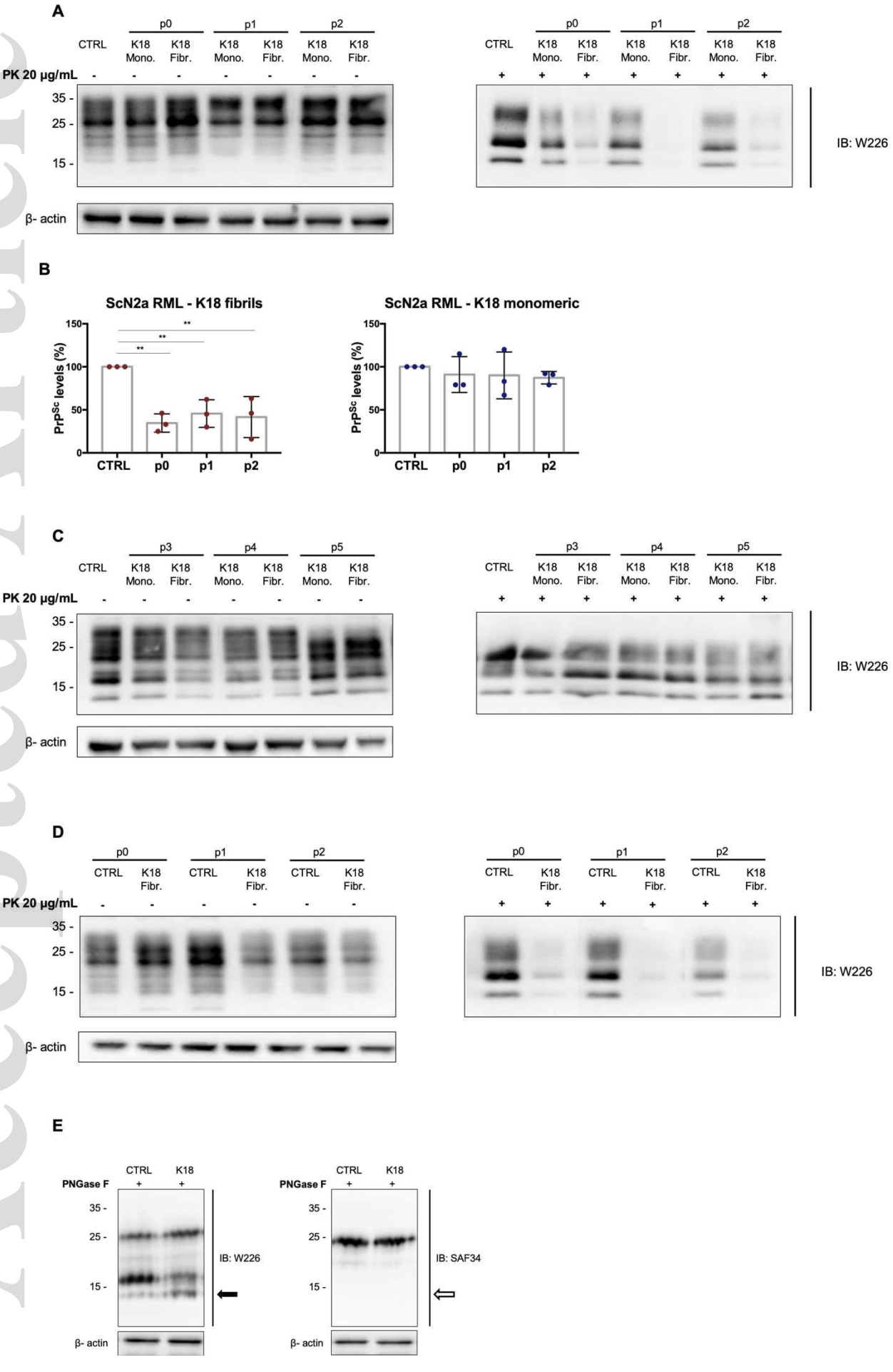

Figure 5. Clearance of PrP^{Sc} from prion-infected ScN2a cell lines after treatment with tau K18 amyloids. (A) Western blot analysis of PK-resistant PrP^{Sc} in ScN2a RML cell lysates upon treatment with tau K18 amyloids for 3 days from the addition of the fibrils (passage 0) to passage 2. (B) Quantification of three independent experiments. Values are shown as a percentage of PK-resistant form relative to β-actin. β-Actin is a loading control. Data are represented as mean ± SD. Data were evaluated by one-way ANOVA with multiple comparisons. Statistical analysis is indicated as: *= $p < 0.05$, **= $p < 0.01$, ***= $p < 0.001$. (C) Western Blot analysis of further passaging of treated cells shown in (A), from passage 3 to passage 5. (D) Western blot analysis of PK-resistant PrP^{Sc} in ScN2a 22L cell lysates upon treatment with tau K18 amyloids for 3 days. (E) Electrophoretic pattern of PNGase F digested PrP in ScN2a control cells and cells treated with tau K18 fibrils. Solid black arrow shows the presence of C1 fragment recognized with C-terminal Ab (W226), while the broken black arrow indicates the absence of the bands when the membrane was probed with N-terminal antibody (SAF34).